J Mater Sci (2013) 48:7134–7141
DOI 10.1007/s10853-013-7529-9

Strain rate-dependant mechanical properties of OFHC copper

Jennifer L. Jordan · Clive R. Siviour · George Sunny · Craig Bramlette · Jonathan E. Spowart

Received: 6 March 2013 / Accepted: 12 June 2013 / Published online: 27 June 2013
© Springer Science+Business Media New York (outside the USA) 2013

Abstract The mechanical properties of high purity copper have been extensively studied in the literature, with yield and flow stresses measured as a function of strain rate, grain size, and temperature. This paper presents a comprehensive study of the strain rate and grain size dependence of the mechanical properties of OFHC copper, including an investigation of the previously observed upturn in rate dependence of flow stress at high rates of strain ($\geq$500 s^{-1}). As well as a comprehensive review of the literature, an experimental study is presented investigating the mechanical properties of OFHC copper across a range of strain rates from 10^{-3} to 10^{5} s^{-1}, in which the copper samples were designed to minimize the effects of inertia in the testing. The experimental data from this study are compared with multiple sources from the literature varying strain rate and grain size to understand the differences between experimental results on nominally the same material. It is observed that the OFHC copper in this study showed a similar increase in flow stress with strain rate seen by other researchers at high strain rates. The major contribution to the variation between experimental results from different studies is most likely the starting internal structure for the materials, which is dependent on cold working, annealing temperature, and annealing time. In addition, the experimental variation within a particular study at a given strain rate may be due to small variations in the internal structure and the strain rate history.

J. L. Jordan (✉) · G. Sunny · C. Bramlette
Air Force Research Laboratory, Eglin AFB, FL 32542, USA
e-mail: jennifer.jordan@afosr.af.mil

C. R. Siviour
Department of Engineering Science, University of Oxford, Parks Road, Oxford, UK

J. E. Spowart
Air Force Research Laboratory, Wright-Patterson AFB, OH, USA

Introduction

The mechanical response of high purity (oxygen-free, high conductivity: OFHC) copper has been extensively studied in the literature as a function of strain rate [1–5], grain size [2, 6–13], and temperature [4, 7, 11, 12, 14, 15]. The flow stress in copper has been shown to be grain size dependent according to the well-known Hall–Petch relationship [16, 17]:

$$\sigma = \sigma_0 + kd^{-1/2} \quad (1)$$

where σ is the stress, σ_0 and k are constants, and d is the average grain size. According to this relationship, the strength of the polycrystalline sample will increase with decreasing grain size, which has been observed experimentally for micron-sized grains [2, 6–8]. However, the grain size dependence of yield strength does not follow the Hall–Petch relationship for nanosized grains [18], where one study postulated a gradual change in deformation mechanism with decreasing grain size [9]. While Iyer et al. [19] observed a linear dependence of flow stress on the inverse square root of particle size for nanosized grains, the Hall–Petch coefficient, k, was considerably smaller than that observed in micron-sized polycrystalline copper. Several authors have observed that grain size may not be an appropriate variable to consider, but rather the average distance between barriers to dislocation motion, e.g., dislocation cell walls [2, 6]. Gourdin and Lassila [8] reported that the Hall–Petch coefficient, k, was constant in the strain rate range 0.001–100 s^{-1}, while Meyers et al. [2] found that the Hall–Petch coefficient, k, increased slightly with

increasing strain rate when measured at low strains and increased more dramatically with strain rate for 20–40 % strain, which they attributed to the rate of dislocation multiplication and other factors.

In order to examine the effects of strain rate on material properties, it is common to compare the stress at a given strain over a range of different rates, and previous studies have shown that such a comparison shows an increase in slope at high strain rates, with the change in slope occurring between 1×10^3 and 2.5×10^4 s^{-1} as reported in [20]. Follansbee [21] has published one of the few studies investigating a single type of copper across a large range of strain rates, the data from this study are shown in Fig. 1, where the upturn in flow stress can be seen; this figure also includes data from shock loading of copper by Swegle and Grady [22] showing that the stress supported by the material demonstrates a significant increase in this regime. The interpretation of the rapid increase in the strain rate dependence of flow stress in copper has been subject to debate. Traditional interpretation of this increase in flow stress has attributed it to the transition between thermally activated and dislocation drag limited dislocation motion at these strain rates [10, 23, 24], which has been argued against by several authors. Armstrong and Zerilli [25] have suggested that the sudden increase in flow stress is due to an enhanced rate of dislocation generation at strain rates exceeding 1000 s^{-1}. Follansbee [21] has suggested that constant dislocation structure should be used, as opposed to constant strain, in the relationship between flow stress and strain rate. The Mechanical Threshold Stress model [8] has this structural state variable as its underlying principle where the instantaneous flow depends on the instantaneous condition of the material as well as strain rate and other state variables, e.g., temperature. Plotting stress versus strain rate at a constant threshold stress, rather than strain, shows no upturn at strain rates up to 10^4 s^{-1} [1].

Gorham [26] proposed that the strain rate increase may be due to differences in deformation velocity, wave propagation, friction and/or inertia, i.e., effects which are primarily associated with sample geometry. Although many of these effects are difficult to quantify, the inertial stress, σ can be approximated from the following equation [20]:

$$\sigma_{\mathrm{i}} = \rho\left(\frac{a^2}{16}+\frac{h^2}{6}\right)\dot{\varepsilon}^2 + \rho\left(\frac{h^2}{6}-\frac{a^2}{8}\right)\ddot{\varepsilon} \qquad (2)$$

where ρ is the specimen density, a is the radius, h is the height, and ε is the strain. In high rate testing, the two terms are usually of similar magnitude, which can have a significant effect on the flow stress.

Constitutive models are used to quantify the relationship between stress, strain, strain rate, temperature, and pressure. Several constitutive models have been developed ranging from the empirical Johnson–Cook model [27] to the structurally dependent Mechanical Threshold Stress (MTS) model [1], with a range of models between these two extremes.

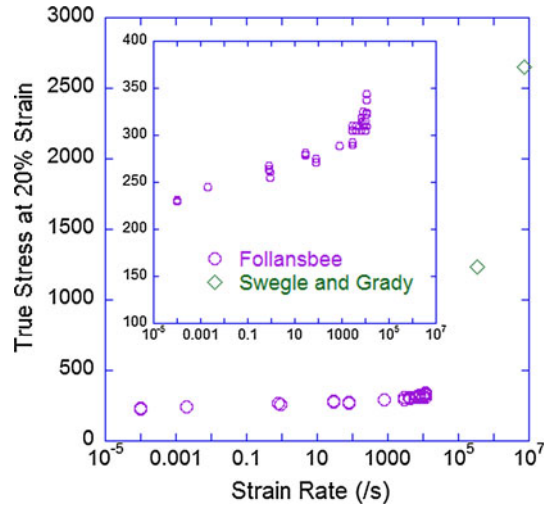

Fig. 1 True stress versus strain rate for copper from Follansbee [21] and Swegle and Grady [22]

As mentioned above, the MTS model accurately captures the upturn in flow stress, which would attribute this property to a change in the underlying structure of the copper. However, this model is complex to implement in material codes and requires the determination of parameters that are difficult or impossible to measure experimentally. Several models are based on the thermal activation of dislocation motion [28–30], where plastic flow is controlled by the motion of athermal long range barriers and thermally-controlled short range barriers, e.g., forest dislocations, point defects, and impurities. However, these models do not adequately capture the upturn in flow stress at a constant strain. To address this issue, models have been developed that incorporate dislocation density evolution to account for the microstructural changes that are occurring in the copper at extremely high strain rates [31, 32] as well as models that incorporate viscous drag [33].

The experimental study presented in this paper investigates the mechanical properties of OFHC copper across a range of strain rates from 10^{-3} to 10^5 s^{-1}, where the copper samples were designed to keep the first term in Eq. (2) approximately constant between samples and to eliminate the second term to minimize the effects of inertia on the data obtained. The experimental data from this study are compared with multiple literature sources varying strain rate and grain size to understand the differences between experimental results on nominally the same material.

Experimental approach

Sample preparation

The copper in this study was obtained from a 12.7 mm diameter rod (Hitachi grade OFE). The samples were

machined to the desired size, and then some were annealed at 350 °C for 1 h and allowed to cool in the oven after it was turned off. The copper was tested in both the as-received and annealed conditions. The sample geometries in this study have been designed to minimize the effects of inertia on the flow stress of the material, see Table 1. Micrographs of the annealed copper samples are shown in Fig. 2. The grain diameters for the annealed samples were measured from both longitudinal and transverse sectioning planes. The grain diameters were observed to be isotropic, with a mean grain size of approximately 35 μm.

Compression testing

Compression experiments were performed across a range of strain rates from 10^{-3} to 10^{4} s^{-1}, at room temperature. A hydraulic load frame with parallel, steel platens was used for quasi-static loading, in which the cylindrical samples were nominally 8.00 mm diameter by 3.50 mm thick. It is generally accepted that quasi-static compression samples should have a length to diameter ratio of 2:1. However, it has been shown that there is little difference between samples tested quasi-statically using 2:1 or 1:2 length:diameter ratio if the correct lubrication is used [34, 35]. In these experiments, samples with dimensions identical to those used for the split Hopkinson pressure bar were tested. Specimens were either lubricated with $MoSi_2$ grease, or placed on a glass-reinforced PTFE sheet between the platens to reduce friction. In all cases, minimal barreling of the specimen was observed. The strain in the sample was determined from crosshead displacement, and the stress was determined from the calibrated load cell output.

Compression experiments at intermediate strain rates ($\sim 10^{3}$ s^{-1}) were conducted using a split Hopkinson pressure bar (SHPB) [36, 37], a schematic diagram of which can be seen in Fig. 3a. The experiments varying strain rate were conducted using the SHPB system located at AFRL/RWME, Eglin AFB, FL, which is comprised of 1524 mm long, 19 mm diameter 440-HT stainless steel incident and transmitted bars. The striker is 305 mm long and made of the same material as the other bars. The samples, which were nominally 8 mm diameter by 3.5 mm thick or 5 mm diameter by 2.5 mm thick, depending on strain rate, are positioned between the incident and transmitted bars. The bar faces were lightly lubricated with grease to reduce friction.

In order to fully understand mechanical properties and material behavior under impact conditions, the response of materials at even higher rates is necessary. The 'traditional' SHPB, extensively discussed by Gray [38], is typically able to characterize the mechanical properties of materials at strain-rates up to about 5×10^{3} s^{-1}. While still higher velocity impacts can be generated using plate-impact experiments (10^{6}–10^{7} s^{-1}), there is still a gap between the two different strain-rate regimes. To fill this gap, a number of researchers have performed similar experiments using a miniaturized split-Hopkinson pressure bar (MSHPB). For example, Jia and Ramesh [39] designed a sophisticated

Table 1 Experimental parameters for testing OFHC copper at varying strain rates using copper density of 8.9 g/cm^3

Diameter (mm)	Length (mm)	Desired strain rate (s^{-1})	Inertial terms (Eq. 2)		SHPB configuration
			$\rho\left(\frac{a^2}{16}+\frac{h^2}{6}\right)\dot{\varepsilon}^2$ (MPa)	$\left(\frac{h^2}{6}-\frac{a^2}{8}\right)$ (m^2)	
8	3.5	1000	0.027	4.2×10^{-8}	19 mm ∅—304 SS
1.5	0.65	10000	0.094	1.0×10^{-10}	3.2 mm ∅—Ti–6Al–4V

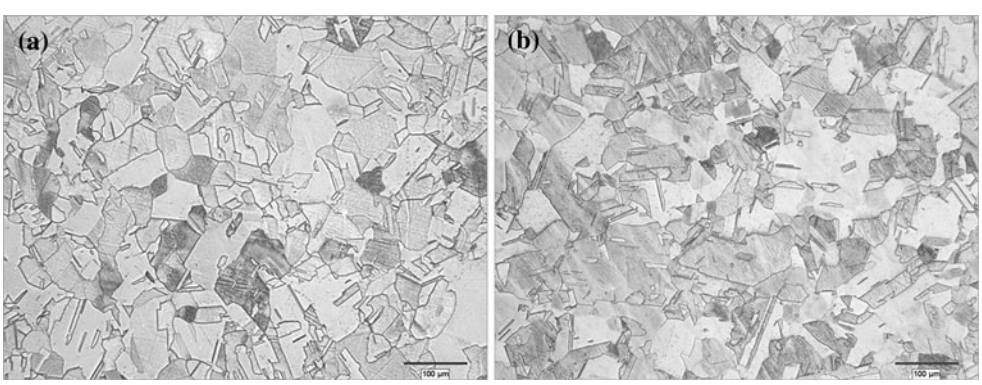

Fig. 2 Microstructure of copper samples in the **a** longitudinal and **b** transverse sample direction showing no preferential alignment of the grains after annealing

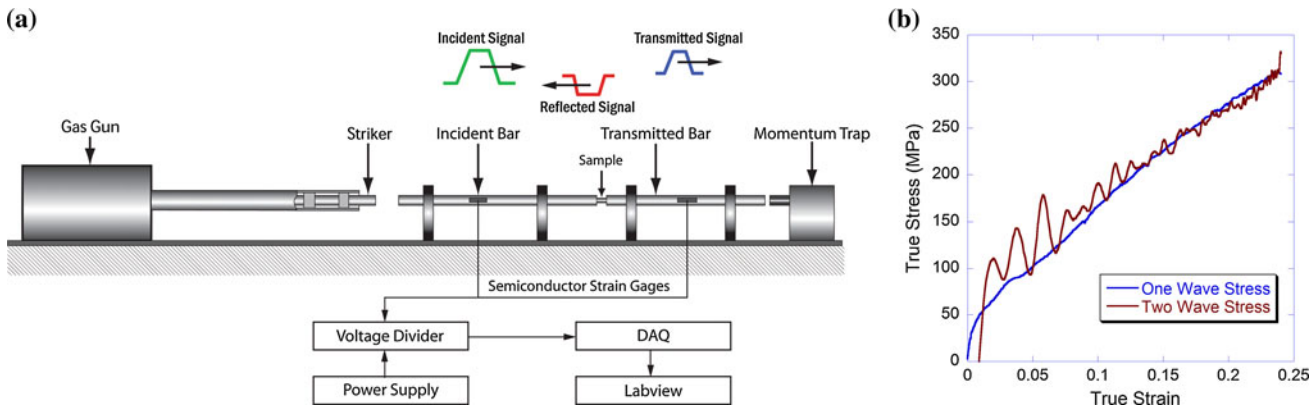

Fig. 3 **a** Schematic and **b** photograph of miniaturized split Hopkinson pressure bar (MSHPB)

MSHPB that incorporates strain control for use in the testing of 6061-T651 aluminum; Casem [40] performed experiments to increase the strain-rate regime to 10^5 s^{-1}. In addition, Jordan et al. [41] have conducted experiments on polytetrafluoroethylene (PTFE), Epon 826/DEA [42], and epoxy–aluminum composites [43] at strain-rates up to 4×10^4 s^{-1} and Nemat-Nasser et al. [44] investigated the behavior of Ni–Ti shape memory alloys to 2×10^4 s^{-1}.

The MSHPB at AFRL/RWME (Fig. 3a) consists of a 100 mm long striker bar, a 300 mm long input (incident) bar, a 300 mm long output (transmitted) bar, and a 150 mm bar that acts as a momentum trap to limit repeated reverberations in the sample. All of the bars have a diameter of 3.2 mm and are made of Ti–6Al–4V. The striker bar is housed inside a PTFE sabot traveling along the inside of a gun barrel. All bars are mounted with PTFE bearings to reduce friction. Operation of the MSHPB is performed by the quick release of air from the firing tank. Upon impact between the striker bar and the input bar, a stress wave is generated and propagated along the input bar (incident pulse). When the stress wave reaches the sample, which is placed in between the input and output bars, some of the wave is reflected back through the input bar (reflected pulse), while the rest of the wave is transmitted into the sample. There, the wave reverberates in the sample to reach stress equilibrium and the wave continues into the output bar (transmitted pulse) and is then absorbed by the momentum trap.

For both the 19 mm ∅ and the 3.2 mm ∅ (miniature) bar systems, the properties of the sample are determined by measuring the incident, reflected, and transmitted strain signals, ε_I, ε_R, and ε_T, respectively, using Kulite AFP-500-90 semiconductor strain gages. These gages are smaller (1 mm long) than traditional foil gages and have a much higher gage factor (140). The gages form part of a potential divider circuit with constant voltage excitation, which transforms the resistance change of the gages to a voltage change and compensates for temperature changes. The strain gages are dynamically calibrated in situ by performing a number of impacts with carefully measured striker bar velocities. From the measured impact velocity and mass of the striker, the force amplitude of the stress pulse introduced, F, can be determined and compared to the voltage output, V, from the strain gages to give a calibration in the form:

$$F = KV(1 + bV), \tag{3}$$

where K and b are calibration factors.

The full derivation of the data reduction used to calculate the strain rate and stress in the specimen, as functions of time, can be found in references [36, 37, 45]. In order to make representative measurements of material properties, it is necessary that the specimen achieves mechanical equilibrium during the experiment, and this is sometimes assumed as it makes the strain rate calculation more straightforward [36]. Equilibrium can be confirmed in practice by calculating the stresses on the front and rear faces of the specimen using the one- and two-wave analyses, respectively, as described by [36]. The software used to analyze the experiments presented in this paper performs the one- and two-wave analyses automatically for every specimen, so stress state equilibrium is verified in every experiment. However, the calculation of strain rate does not assume mechanical equilibrium, rather it uses all three of the incident, reflected and transmitted force pulses to calculate specimen strain rate through the following equation:

$$\dot{\varepsilon}(t) = \left[\frac{C_b}{l_s}\right](\varepsilon_I(t) - \varepsilon_R(t) - \varepsilon_T(t)), \tag{4}$$

where ε_I, ε_R, and ε_T are the incident, reflected and transmitted strain pulses time shifted to the front and rear faces of the specimen, respectively, C_b is the sound speed in the bar material, and l_S is the length of the sample. This specimen strain rate is then integrated to give the strain,

$$\varepsilon(t) = \int_0^t \dot{\varepsilon}(t)\mathrm{d}t, \tag{5}$$

and the transmitted strain pulse is used to calculate the reported one-wave specimen stress,

$$\sigma(t) = \left[\frac{E_b A_b}{A_S}\right]\varepsilon_T(t), \tag{6}$$

where E_b, and A_b are the elastic modulus and cross-sectional area of the bar material, respectively, and A_s is the cross-sectional area of the sample. The two-wave specimen stress is calculated using Eq. 4 with ε_T replaced by $\varepsilon_I + \varepsilon_R$. If true stress is required, A_S is typically updated using the strain calculation, assuming that volume is conserved during deformation. As discussed above, stress equilibrium is verified during each test and a representative one wave—two wave analysis is shown in Fig. 3b, where the oscillation of the two wave stress about the one wave stress at a low strain ($\sim$0.05) indicates that the samples are in equilibrium at these very high strain rates.

In order to confirm volume conservation, the changing diameters of the expanding copper specimens were measured in situ on an SHPB at the University of Cambridge, UK using laser diameter measurement [46, 47]. The radial expansion measurements can be used to test the constant volume assumption of the SHPB equations. The Poisson's ratio, ν, during the experiment can be calculated by:

$$\nu = \frac{\varepsilon_r}{\varepsilon_a}, \tag{7}$$

where ε_r and ε_a are the radial and axial strains, respectively. This is a pragmatic engineering extension of the Poisson's ratio, which is only defined for small elastic strains. The Cambridge SHPB system uses the same gages and data reduction as the 19 and 3.2 mm ∅ (miniature) bar systems discussed above.

Results and discussion

The mechanical response of the as received copper as a function of strain rate is shown in Fig. 4. A sharp transition at yield is observed due to the work hardening during processing. In addition, the as received copper shows strain rate dependence with stress at a given strain increasing with increasing strain rate. Representative stress–strain curves for annealed copper across a range of strain rates are shown in Fig. 5. Again, strain rate dependence is observed in the annealed samples. It has been observed in previous studies that increasing the strain rate results in an increased work hardening rate [1, 2], which is also the case in these experiments. Follansbee and Kocks [1] postulate that at low strain rates dislocations become immobilized and stored after traveling a distance proportional to the average dislocation spacing, leading to a linear increase in strain hardening rate. However, at higher strain rates, the dislocations are only permitted to travel during the time duration of the experiment resulting in considerably less movement that in quasi-static experiments at the same strain, which would give rise to an increased linear strain rate dependence than at low strain rates [1], as well as providing an estimate of dislocation speed.

The measurements of radial and longitudinal strain measured using a laser diameter measurement system along with a photographic technique are presented in Fig. 6. The solid points were measured using the laser diameter measurement system and the open points were measured using high speed photographs of the deforming sample. In all cases, the ratio between radial strain and longitudinal strain is an approximately constant value, 0.5 ± 0.1, which is consistent with the sample having yielded and subsequently flowed at constant volume, thereby supporting the use of volume conservation in the calculation of true specimen stress.

In order to quantify the dependence of flow stress on strain rate, the true stress at 20 % strain was plotted as a function of strain rate in Fig. 7. The dependence on strain rate is linear with a gradual slope up to $\sim 3 \times 10^3$ s^{-1} and, then, shows the dramatic upturn in stress seen by Follansbee [21], as seen in Fig. 1. To compare with the literature values on high purity copper, the annealed data from this study is plotted in Fig. 8 along with data from several sources in the literature [2–4, 8, 12, 14, 21, 48]. There is considerable scatter in the data from different sources although all data is measured on high purity copper.

One source of the scatter is grain size. This is particularly evident in the low strain rate data of Hansen and Ralph [12] and Gourdin and Lassila [8] which were experiments conducted at a single strain rate on multiple grain sizes of copper. In Fig. 9, the stress at 20 % strain for

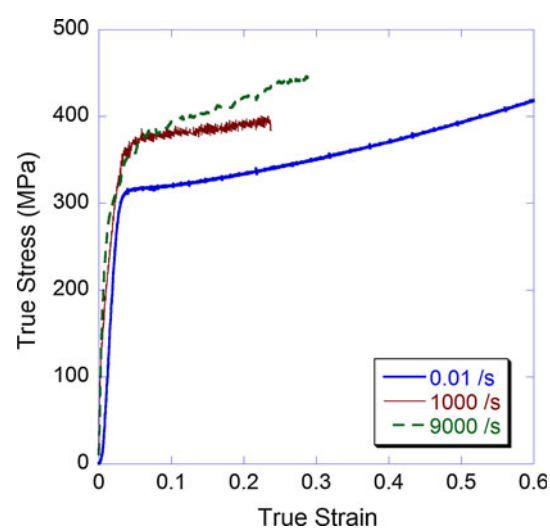

Fig. 4 As received copper stress–strain curves, where the 0.01 and 1000 s^{-1} curves were obtained from 8 mm diameter samples and the 9000 s^{-1} curve was obtained from 1.5 mm diameter samples

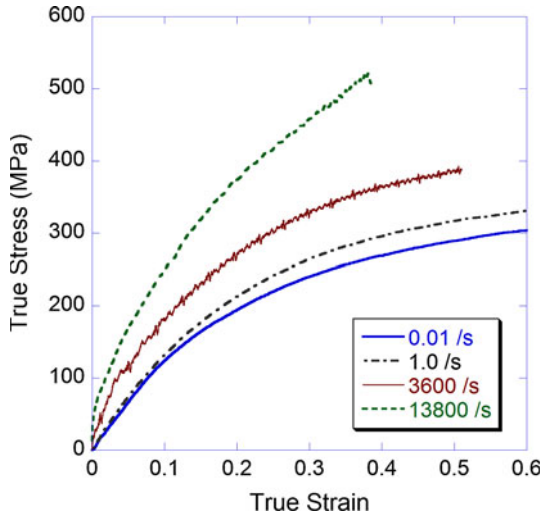

Fig. 5 Annealed copper stress–strain curves, where the 0.01, 1, and 3600 s^{-1} curves were obtained from 8-mm diameter samples and the 9000 s^{-1} curve was obtained from 1.5-mm diameter samples

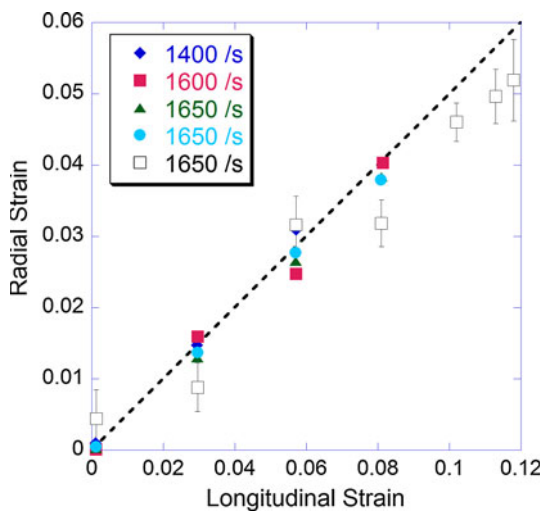

Fig. 6 Radial strain versus longitudinal strain for annealed copper revealing a ratio of 0.5 between radial strain and longitudinal strain under dynamic loading confirming conservation of volume during the experiment. The *close symbols* are from the laser diameter measurement system and the *open symbols* are from photographic measurement

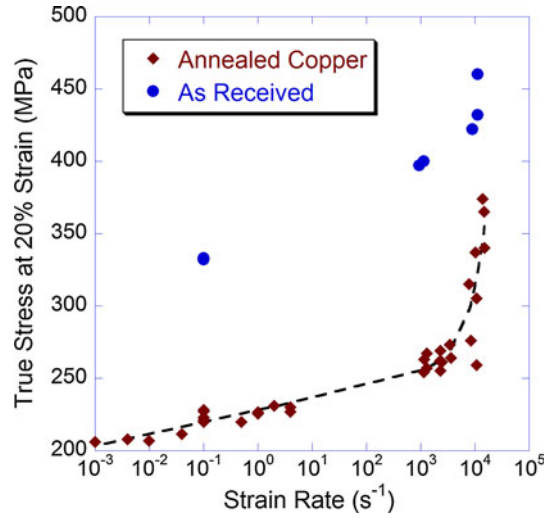

Fig. 7 As received and annealed copper strain rate–stress curves, showing an increase in flow stress with strain rate

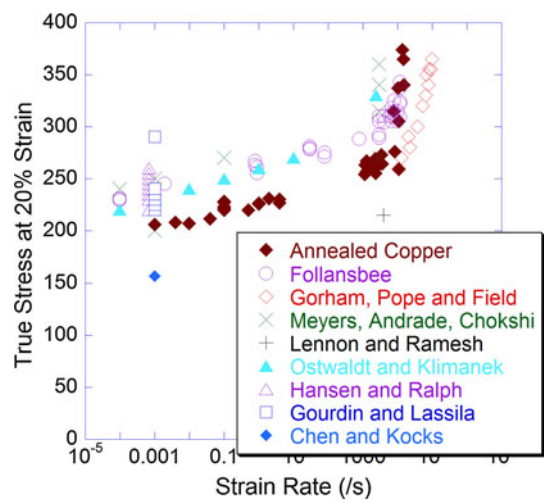

Fig. 8 True stress at 20 % strain for annealed copper from this study compared with data from the literature for Follansbee [21]; Gorham et al. [3]; Meyers et al. [2]; Lennon and Ramesh [14]; Ostwaldt and Klimanek [4]; Hansen and Ralph [12]; Gourdin and Lassila [8]; and Chen and Kocks [48]

data from this study as well as data from the literature [2, 4, 8, 12, 21] is plotted versus the inverse square root of grain size, d, to determine the coefficient, k, in Eq. 1. At low strain rates, $\sim$0.001 s^{-1}, the coefficient is 4.49 MPa $mm^{1/2}$ and at high strain rates, $\sim$3000 s^{-1}, the coefficient is 3.65 MPa $mm^{1/2}$. These values are in agreement with those reported in the literature at 20 % strain by Meyers et al. [2]: 0.75–2.6 MPa $mm^{1/2}$; Armstrong and Zerilli [24]: 5 MPa $mm^{1/2}$; Gourdin and Lassila [8]: 2.78 MPa $mm^{1/2}$; Feltham and Meakin [49]: 3.53 MPa $mm^{1/2}$; Ono and Karashima [7]: 2 MPa $mm^{1/2}$; and Hansen and Ralph [12]: 4.5 MPa $mm^{1/2}$. Of all the references sited, only Meyers et al. [2] and Gourdin and Lassila [8] considered the effect of strain rate on k, although Gourdin and Lassila considered a much narrower range of strain rates.

Based on their measurements, Gourdin and Lassila [8] conclude that the flow stress is composed of a grain size dependent part, which is independent of strain and strain rate and an evolutionary part that is dependent on both. By subtracting the grain size effect from the flow stress, one should be able to collapse the copper data onto a "master curve," where the stress for a given grain size could be found simply by adding in the grain size effect. In Fig. 10, the low strain rate coefficient equal to 4.49 MPa $mm^{1/2}$ was used to "collapse" the data. It can be seen that the

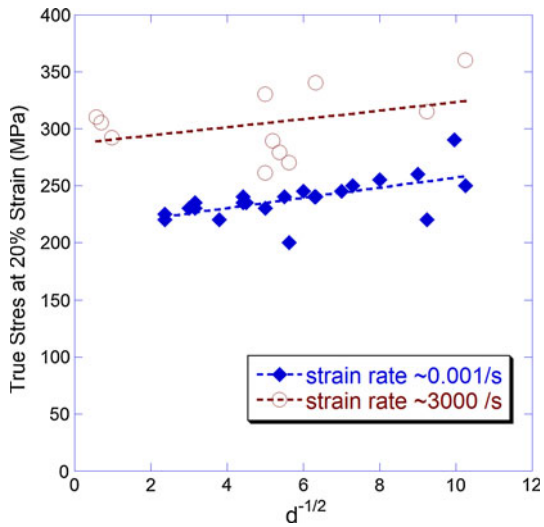

Fig. 9 True stress at 20 % strain versus the inverse square root of grain size (d) at two strain rates to determine the coefficient k in Eq. (1). The slope of the line at $\sim 0.001\ s^{-1}$ is 4.49 MPa $mm^{1/2}$ and the slope at $\sim 3000\ s^{-1}$ is 3.65 MPa $mm^{1/2}$. Data from this study are included along with that of Refs. [2, 4, 8, 12, 21]

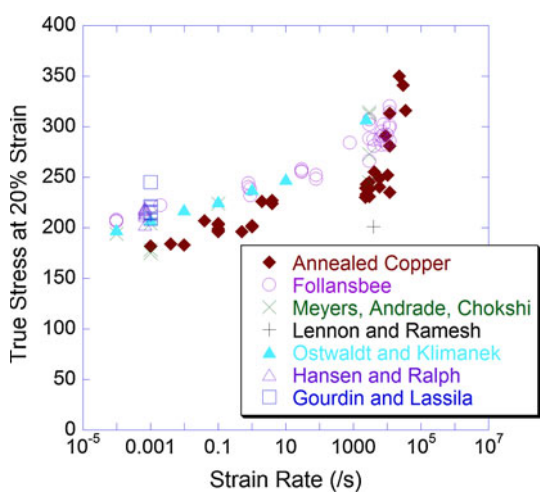

Fig. 10 True stress at 20 % strain for annealed copper from this study with the grain size effect subtracted from the data to create a "master curve" compared with data from the literature for Follansbee [21]; Meyers et al. [2]; Lennon and Ramesh [14]; Ostwaldt and Klimanek [4]; Hansen and Ralph [12]; and Gourdin and Lassila [8]

scatter from Fig. 8 is reduced, although not entirely eliminated, suggesting the need for continued investigation into the sources of differences between flow stress data collected from nominally similar materials.

There are several additional reasons for differences in data measured on the same type of copper by different researchers. Gorham [20] discussed several sources of experimental variation that should be considered. He observed that the strain rate at which the upturn in flow stress occurred varied from researcher to researcher and was dependant on the size of the specimen used. He considered inertia as a cause for the specimen size dependence, and while he showed not likely to be significant for the specimen sizes that had been used previously in the literature, his analysis also shows the importance of considering specimen size when designing high rate experiments. The specimen dimensions in the current study were designed to keep the inertial contributions constant as a function of strain rate. Gorham did postulate that wave dispersion in the bar resulting in a rise time on the order of microseconds may play a role in the specimen size dependence of the upturn strain rate. These experimental sources of error may contribute to the variations seen between the multiple sources of data in Fig. 10, where the sample dimensions, bar systems, and lubrication vary from laboratory to laboratory.

The final reason that must be investigated is the role of constant structure versus constant strain that is discussed by Follansbee [21]. Each of the copper samples investigated in the literature was subjected to different processing conditions prior to testing, including cold working, annealing temperature, and annealing time. In addition, the structure at a given strain is dependent on the grain size of the starting material, as seen by Gracio et al. [50] where increasing grain size resulted in increased dislocation cell size. The transition between large and small grain materials is $\sim$65–250 μm. The dislocations in small grained materials are greatly influenced by the surroundings resulting in many geometrically necessary dislocations. Follansbee [21] has shown that plotting the true stress as a function of strain rate for a constant mechanical threshold stress results in a linear relationship, giving much credence to the theory that structure, rather than strain, needs to be the state variable. However, the experiments to determine constant structure require considerably more effort that traditional stress–strain tests, and the data are not available for all of the sources presented in Fig. 10. This difference in structure is believed to be the reason that the experimental data from the present study lies on a lower—although parallel—curve to the much of the literature data. The materials from each study were processed differently giving rise to a varied internal structure at the initiation of the experiment.

It can be seen both from the present study and from Follansbee's work [9] that there is considerable variation within a particular set of samples at a given strain rate, particularly when that strain rate is greater than $10^3\ s^{-1}$. This variation may also be attributed to the internal structure, which may vary from sample to sample, and also the strain rate history, which may not be identical from test to test.

Conclusions

This paper presented a review of the literature on the strain rate and grain size dependence of mechanical properties in

copper. In addition, sources for the upturn in flow stress versus strain rate were discussed. The experimental study presented investigated the mechanical properties of OFHC copper across a range of range of strain rates from 10^{-3} to 10^{5}, where the copper samples were designed to minimize the effects of inertia in the testing. The OFHC copper tested showed an increase in flow stress with strain rate and duplicated the upturn seen by other researchers at high strain rates.

The experimental data from this study is compared with multiple literature sources varying strain rate and grain size to understand the differences between experimental results obtained from nominally the same material. The first source of variation investigated was grain size, where subtracting out the grain size effect using the Hall–Petch relationship decreased the scatter in the experimental data. Experimental sources of error as identified by Gorham [14] may contribute to the variations seen between the multiple sources of data in Fig. 10, where the sample dimensions, bar systems, and lubrication vary from laboratory to laboratory. The major contribution to the variation between experimental results from different studies is most likely the starting internal structure for the materials, which is dependent on cold working, annealing temperature, and annealing time. In addition, the experimental variation within a particular study at a given strain rate may be due to small variations in the internal structure and the strain rate history.

Acknowledgements The authors would like to acknowledge Mr. William (Tony) Houston (UES, Inc.) for preparing the metallographic specimens and obtaining the photomicrographs of the copper samples, and Mr. Ronald E. Trejo, Mr. John D. Camping, and Ms. Alysa J. Scherer (UDRI) for assisting with low- and medium-rate mechanical testing.

References

1. Follansbee PS, Kocks UF (1988) Acta Metall 36(1):81
2. Meyers MA, Andrade UR, Chokshi AH (1995) Metall Mater Trans A 26A(11):2881
3. Gorham DA, Pope PH, Field JE (1992) Proc R Soc A 438:153
4. Ostwaldt D, Klimanek P (1997) Mater Sci Eng A A234–A236:810
5. Kvackaj T et al (2010) Mater Lett 64:2344
6. Miyazaki S, Fujita H (1978) Trans Jpn Inst Met 19(8):438
7. Ono N, Karashima S (1982) Scr Metall 16:381
8. Gourdin WH, Lassila DH (1991) Acta Metall Mater 39(10):2337
9. Gertsman VY et al (1994) Acta Metall Mater 42(10):3539
10. Kumar A, Kumble RG (1969) J Appl Phys 40(9):3475
11. Tanner AB, McDowell DL (1999) Int J Plast 15:375
12. Hansen N, Ralph B (1982) Acta Metall 30:411
13. Mishra A et al (2008) Acta Mater 56:2770
14. Lennon AM, Ramesh KT (2004) Int J Plast 30:269
15. Samanta SK (1971) J Mech Phys Solids 19:117
16. Petch NJ (1953) J Iron Steel Inst 174(1):25
17. Hall EO (1951) Proc Phys Soc B64(9):747
18. Chokshi AH et al (1989) Scr Metall 23:1679
19. Iyer RS et al (1999) Mater Sci Eng A A264:210
20. Gorham DA (1989) J Phys D Appl Phys 22:1888
21. Follansbee PS (2001) In: Murr LE, Staudhammer KP, Meyeres MA (eds) Metallurgical applications of shock-wave and high-strain-rate phenomena. Marcel Dekker, Inc., New York, pp 451
22. Swegle JW, Grady DE (1985) J Appl Phys 58(2):692
23. Follansbee PS, Regazzoni G, Kocks UF (1984) In: Harding J (ed) Mechanical properties of materials at high strain rates. The Institute of Physics, London, pp 71
24. Armstrong RW, Zerilli FJ (1988) J Phys C3 49(9):529
25. Armstrong RW, Zerilli FJ (2001) In: Staudhammer LEMKP, Meyers MA (eds) Fundamental issues and applications of shock-wave and high-strain-rate phenomena. Elsevier Science Ltd, Amsterdam, pp 115
26. Gorham DA (1991) J Phys D Appl Phys 24:1489
27. Johnson GR, Cook WH (1983) In: Proceedings of the 7th international symposium on ballistics. International Ballistics Committee, The Hague
28. Gao CY, Zhang LC (2010) Mater Sci Eng A 527:3138
29. Armstrong RW, Arnold W, Zerrilli FJ (2009) J Appl Phys 105:023511
30. Nemat-Nasser S, Li Y (1998) Acta Mater 46(2):565
31. Gao CY, Zhang LC (2012) Int J Plast 32–33:121
32. Voyiadjis GZ, Abed FH (2005) Mech Mater 37:355
33. Rusinek A, Rodriguez-Martinez JA, Arias A (2010) Int J Mech Sci 52:120
34. Chen W, Zhang X (1997) J Eng Mater Technol Trans ASME 119(3):305
35. Li P, Siviour CR, Petrinic N (2009) Exp Mech 49:587
36. Gray GT III (2002) In: Kuhn H, Medlin D (eds) ASM handbook. Mechanical testing and evaluation, vol 8. ASM International, Materials Park, pp 462
37. Tasker DG, Dick RD, Wilson WH (1998) In: Shock compression of condensed matter—1997. American Institute of Physics
38. Gray GT (2000) In: Kuhn H, Medlin D (eds) ASM handbook: mechanical testing and evaluation, vol 8. ASM International, Materials Park, pp 462
39. Jia J, Ramesh KT (2004) Exp Mech 44(5):445
40. Casem DT (2009) In: Society for Experimental Mechanics Conference. Albuquerque
41. Jordan JL, Siviour CR, Foley JR, Brown EN (2007) Polymer 48(14):4184
42. Jordan JL, Foley JR, Siviour CR (2008) Mech Time Depend Mater 12(3):249
43. Jordan JL, Siviour CR, Richards DW, Rumchik CG, Dick RD (2005) In: Society for Experimental Mechanics Conference. Portland
44. Nemat-Nasser S et al (2007) Mech Mater 37:287
45. Tasker DG, Dick RD, Wilson WH (1997) In: Shock compression of condensed matter—1997. American Institute of Physics
46. Ramesh KT, Narasimhan S (1996) Int J Solids Struct 33(25):3723
47. Siviour CR et al (2005) Polymer 46:12546
48. Chen SR, Kocks UF (1991) High-temperature plasticity in copper polycrystals. Los Alamos National Laboratory, Los Alamos
49. Feltham P, Meakin JD (1957) Phil Mag 2(13):105
50. Gracio JJ, Fernandes JV, Schmitt JH (1989) Mater Sci Eng A A118:97